Journal of Materials Chemistry B

Accepted Manuscript

ROYAL SOCIETY OF CHEMISTRY

www.rsc.org/materialsB

Journal of Material Chemistry B RSCPublishing

ARTICLE

Miktoarm star conjugated multifunctional gold nanoshells: synthesis and an evaluation of biocompatibility and cellular uptake

Cite this: DOI: 10.1039/x0xx00000x

Received 00th January 2012,
Accepted 00th January 2012

DOI: 10.1039/x0xx00000x

www.rsc.org/

Vanessa W.K. Ng,[a,‡] Pramod K. Avti,[a,b,c,‡] Mathieu Bedard,[a] Tina Lam,[a] Leonie Rouleau,[b,c,d] Jean-Claude Tardif,[c,e] Eric Rhéaume,[c,e,*] Frederic Lesage[b,c,*] and Ashok Kakkar[a,*]

Simple and highly versatile click chemistry based synthetic strategy to develop an ABC type miktoarm star ligand that is conjugated to gold nanoshells (GNS), is reported. The surface functionalized multifunctional GNS contain lipoic acid (LA) as a model therapeutic, poly(ethylene glycol) (PEG_{350}) as solubilizing and stealth agent, and tetraethylene glycol (TEG) with a terminally conjugated thiol moiety. These GNS have an average size of 40 nm, shell thickness of 6 nm, a well-defined crystal structure lattice (111), and a surface absorption plasmon band in the near infrared (NIR) region. Miktoarm star and GNS functionalized with this ligand are non-cytotoxic for up to 5 μg/mL concentrations, and human umbilical vein endothelial cells internalize more than 85% of these GNS at 5μg/mL. Our results establish that biocompatible miktoarm star ligand provides a useful platform to synthetically articulate the introduction of multiple functions onto GNS, and enhance their scope by combining their inherent imaging capabilities with efficient delivery and accumulation of active therapeutic agents.

1. Introduction

Gold nanoshells (GNS) are emerging as promising tools for biomedical applications due to their unique physicochemical properties and optical characteristics,[1] which may be tuned by modifications of their shell size, shape, thickness and inter-particle distance.[2] Various methods have been developed to synthesize GNS using core-shell systems, with cores composed of silica, silver or cobalt.[3] In 2006, Schwartzberg et al reported a general method for the synthesis of hollow GNS using cobalt as sacrificial template.[4] The labile citrate ions adsorbed on to the GNS surface,[5] and their replacement by thiols which have higher affinity for gold, have provided a useful strategy to link them with a variety of biomacromolecules such as lipids, RNA, DNA, peptide, antibodies, viruses and drugs.[1a,6] To fully exploit the potential of these GNS based nanocarriers, there remains a need for the development of versatile ligands through which a number of desired functional groups including stealth, solubilizing, targeting and therapeutic agents, could be easily incorporated onto GNS.[7]

Miktoarm stars[8] offer an interesting and intriguing platform to develop multifunctional ligands for subsequent conjugation to GNS. These ensembles can be used to introduce different functionalities into a single unit, and could help enhance the scope of GNS based photoacoustic imaging contrast agents.[1a] Much emphasis has been placed recently to develop synthetic methodologies to miktoarm stars with desired architecture.[9] The inclusion of "click" chemistry, which can be applied to a wide range of substrates under mild reaction conditions,[8,10] has expanded the synthetic versatility of miktoarm stars to a variety of applications.[11] We report herein click chemistry based synthetic strategy for the construction of a miktoarm molecular architecture containing lipoic acid as a model therapeutic agent, polyethylene glycol for water solubility, enhanced circulation times and stealth, and a tetraethylene glycol (TEG) arm with a terminal thiol group which is subsequently used for conjugation to GNS. Endothelial dysfunction-associated diseases such as hypertension, atherosclerosis, hyperlipidemia and diabetes, are known to involve complex processes including oxidative stress mediated mechanisms for the vascular complications.[12] Alpha-lipoic acid (α-LA), among other natural compounds, is of growing interest, either as a dietary supplement or a therapeutic agent in the treatment of cardiovascular diseases.[13,14] It is known to have antioxidant and anti-inflammatory properties,[15] and acts as an essential cofactor for many enzymes and is readily taken up by cells where it is reduced to its potent dithiol form.[16] LA has been shown to protect endothelial cells expressing caspase-induced hyperpermeability, by reducing the formation of reactive oxygen species and thereby inhibiting apoptosis.[17,18]

A detailed evaluation of the ligand packing density on the surface of GNS, cytotoxicity, cellular localization and intracellular uptake characteristics, is also reported.

Collectively, our studies demonstrate that miktoarm star and GNS functionalized with this ligand are noncytotoxic and do not induce any morphological changes to HUVEC cells. The functionalized GNS are easily uptaken by these cells, and offer an interesting platform to develop multifunctional nanocarriers which can deliver large amounts of active therapeutic agents such as lipoic acid.

2. Experimental

2.1 Materials and Methods

All reagents purchased from Sigma Aldrich, Fluka,, Alfa Aesar, AK Scientific Inc., ACP Chemicals and Fisher Scientific were used as received, and the details are provided in the Supporting Information. Acetonitrile was dried using calcium hydride, and ultrapure water used in the synthesis was doubly distilled by reverse osmosis through a Millipore RiOS 8 followed by filtration through a MilliQ Academic A10 unit.

NMR: NMR spectra were obtained using 300, 400 or 500MHz Varian Mercury, operated using VNMRJ 2.2D software under LINUX Red Hat 5. Mass spectra were collected using a Kratos MS25RFA high-resolution mass spectrometer in the electrospray ionization (ESI) mode with the sample prepared by dilution to 0.1 mg/mL.

UV-Vis spectroscopy: UV-Vis spectra of GNS and functionalized GNS were recorded at room temperature using the Cary 500 UV-Visible Spectrometer.

Transmission electron microscopy: For TEM analysis, samples were drop-cast and evaporated overnight on to CF400-Cu carbon film on 400 square mesh copper grids (Electron Microscopy Sciences), washed three times with water and stained using a 2% uranyl acetate staining solution. The FEI Tecnai 12 TEM with AMT XR80C CCD Camera was used to obtain TEM images which were in bright-field mode at an accelerating voltage of 120 kV between 6-150 kx magnification. Post-processing image analysis of the TEM images to determine nanoshell probe physical characteristics were carried out using ImageJ software.

Thermogravimetric analysis: TGA Q500 V6.7 Build 203 was used to quantify ligand coverage on GNS. Gold nanoshell probe solutions were lyophilized overnight to completely remove water, and approximately 0.5-3 mg of sample was weighed into a platinum pan for each trial. Runs started with a 10ºC/min ramp to 100ºC, held for 10 minutes in isotherm, ramped up to 650ºC at 5ºC/min, and then held again in isotherm for 5 minutes. Air and N_2 flow rates were set at 40 and 60 mL/min, respectively. The number of miktoarm ligands conjugated to the GNS surface was determined using the weight loss measurements using the following equations: $N_{ligands} = M_{org}/M_w$ x NA (Eq. 1); $N_{nanoshells} = M_{Au}/M_{GNS}$ (Eq. 2); $N_{ligands/AuNS} = N_{ligands}/N_{GNS}$ (Eq. 3); $F_l = SA_{GNS}/N_{ligands/GNS}$ (Eq. 4); $d_p = 1/F_l$, where $N_{ligands}$ is the total number of ligands on the GNS, M_{org} is the assumed mass of organics, M_w is the molecular weight of the given ligand, N_A is the Avagadro's number, M_{GNS} is the mass of single gold nanoshell, $N_{ligands/GNS}$ is the number of ligands per gold nanoshell, F_l is the average ligand footprint, d_p is the packing density.

2.2 Synthesis of the miktoarm star: General: Monotosylated tetraethylene glycol, TEG-Ts (**1**), tetraethylene glycol thioacetate (TEG-SAc, (**2**)), and PEG_{350}-azide (**6**) were prepared by an adaptation of literature procedures.[19,20] Conversion of the 3-bromo-5-iodo benzoic acid to 3-bromo-5-iodo benzyl alcohol, and subsequent Sonogashira coupling reactions to yield TiPS and TMS protected alkynes in the core molecule **7**, and deprotection to remove TMS (**8**) and TiPS (**10**), were carried out using previously published procedures.[8,21]

2.2.1 Mesylated-TEG-Thioacetate, $(O)_2$S-TEGSAc (**3**): Tetraethylene glycol thioacetate (0.237 g, 0.939 mmol) was dissolved in 3 mL of dichloromethane (DCM), and the reaction flask was placed in an ice/water bath. Methanesulphonyl chloride (0.146 mL, 1.88 mmol) was added by syringe and needle while the solution was stirring, followed by the dropwise addition of triethylamine (0.286 mL, 2.07 mmol). The resulting solution turned dark orange in color, and it was left to stir overnight at room temperature. It was subsequently washed first with brine and then MilliQ water, dried over $MgSO_4$, filtered, and the solvent was removed in vacuo, yielding an orange oil (304 mg, 97% yield). ^{1}H NMR (400MHz, $CDCl_3$): δ 2.33 (3H, s, -COC$\underline{H}_3$), 3.08 (3H, s, -OSO$_2$C$\underline{H}_3$), 3.09 (2H, t, -C$\underline{H}_2$S-), 3.57-3.67 (10H, m, -C$\underline{H}_2$C$\underline{H}_2$O-), 3.77 (2H, t, -O$_2$SOC$\underline{H}_2$-), 4.39 (2H, t, -OC$\underline{H}_2$CH$_2$S-) ppm. ^{13}C{^{1}H} NMR (300MHz, $CDCl_3$): δ 28.76 (-CO$\underline{C}$H$_3$), 30.57 (-$\underline{C}$H$_2$S-), 37.70 (-OSO$_2\underline{C}$H$_3$), 69.01-70.62 (7C, -$\underline{C}$H$_2\underline{C}$H$_2$O-), 195.50 (-$\underline{C}$OCH$_3$) ppm. Expected mass: 330.42 g/mol, ESI: m/z = 353.20 [M+Na]$^+$.

2.2.2 Azidified TEG unit, N_3TEGSAc (**4**): The mesylated TEG (**3**) (0.304 g, 0.920 mmol) was dissolved in 1 mL of dimethylformamide (DMF). Sodium azide (0.179 g, 2.76 mmol) was added to the solution while stirring, followed by tetrabutylammonium iodide (TBAI) (0.00680 g, 0.00184 mmol). The reaction mixture was left to stir overnight at 50°C, and then washed with 1 M HCl (10 mL), followed by 1M NaOH (10 mL). DCM was added to the solution mixture, and then washed four times with MilliQ water to remove DMF. After drying the solution over $MgSO_4$, the solvent was removed in vacuo, and the final product was obtained as an orange-yellow oil (0.217 g, 85% yield). ^{1}H NMR (400MHz, $CDCl_3$): δ 2.33 (3H, s, -COC$\underline{H}_3$), 3.09 (2H, t, -C$\underline{H}_2$S-), 3.40 (2H, t, N$_3$C$\underline{H}_2$-), 3.58-3.68 (12H, m, -C$\underline{H}_2\underline{C}H_2$O-) ppm. ^{13}C{^{1}H} NMR (300MHz, $CDCl_3$): δ 28.82 (-CO$\underline{C}$H$_3$), 30.57 (-$\underline{C}$H$_2$S-), 50.66 (N$_3\underline{C}$H$_2$-), 69.60-70.69 (6C, -$\underline{C}$H$_2\underline{C}$H$_2$O-), 195.57 (-$\underline{C}$OCH$_3$) ppm. Expected mass: 277.34 g/mol, ESI: m/z = 300.18 [M+Na$^+$].

2.2.3 Linking of the PEG arm (**9**): Compound **8** (0.600 g, 1.92 mmol) was weighed into a round bottom flask with a stir bar, and PEG-azide (**6,** 0.561 g, 0.154 mmol) dissolved in 3mL THF, and sodium ascorbate (0.038 g, 0.192 mmol) were added. $CuSO_4$ (0.0240 g, 0.096 mmol) dissolved in 1mL H_2O was then added drop wise. A brown color was quickly noticed, and the reaction mixture was left to stir overnight. THF was subsequently removed under vacuum, and the residue washed once with brine and then with water. The product was purified

on a silica column using pure DCM first, and then increasing the polarity using 5% MeOH–DCM mixture to collect the yellow/brown band. The final product was obtained as an orange oil after removing the solvent in vacuo (759 mg, 54% yield). ^{1}H NMR (300 MHz, $CDCl_3$): δ 1.13 (18H, m, TiPS(C$\underline{H}_3$)), 1.85 (1H, td, -OH), 3.35 (3H, m, -$CH_2OC\underline{H}_3$), 3.47-3.64 (24H, m, -C$\underline{H}_2$C$\underline{H}_2$O-), 3.90 (4H, t, -C$\underline{H}_2CH_2$triaz-), 4.60 (4H, t, -C$\underline{H}_2$triaz-), 4.71 (2H, s, -ArC$\underline{H}_2$OH), 7.43 (1H, s, -Ar(C$\underline{H}$)-), 7.83 (1H, s, -Ar(C$\underline{H}$)-), 7.93 (1H, s, -Ar(C$\underline{H}$)-), 8.16 (2H, s, -triaz(CH)-). ^{13}C NMR (300MHz, $CDCl_3$): δ 11.24, 11.29, 18.64, 18.69, 44.62, 50.47, 69.59-70.45, 104.99, 124.05, 128.07, 129.90, 134.61.

2.2.4 Linking the TEGylated arm (**11**): Compound **10** with the PEGylated arm and a free acetylene (0.481 g, 0.922 mmol) was added to 1 equivalent of N_3TEGSAc (**4**) (0.256 g, 0.922 mmol) dissolved in 1.5 mL THF in a round bottom flask with a stir bar. Sodium ascorbate (0.0183 g, 0.0922 mmol) was added to the solution, followed by dropwise addition of $CuSO_4$•$5H_2O$ (0.0115 g, 0.0461 mmol) dissolved in 1.5 mL H_2O. The mixture was then left to stir overnight at room temperature. Silica column purification was carried out using DCM and 10% MeOH, and the product was obtained as an orange/peach colored oil (0.448 g, 60% yield). ^{1}H NMR (400 MHz, $CDCl_3$): δ 1H NMR (300 MHz, $CDCl_3$): δ 2.30 (3H, s, -COC$\underline{H}_3$), 3.01 (2H, t, C$\underline{H}_2$SCOCH$_3$), 3.36 (3H, m, -$CH_2OC\underline{H}_3$), 3.49-3.64 (35H, m, -C$\underline{H}_2$C$\underline{H}_2$O-), 3.94 (4H, d, -C$\underline{H}_2CH_2$triaz-), 4.62 (4H, d, -C$\underline{H}_2$triaz-), 4.82 (2H, s, -ArC$\underline{H}_2$OH), 7.89 (3H, s, -Ar(C$\underline{H}$)-), 8.26 (2H, s, -triaz(CH)-). ^{13}C NMR (300MHz, $CDCl_3$): δ 28.69, 30.51, 50.33, 58.94, 64.40, 69.35-70.51, 71.80, 104.41, 121.54, 123.45, 123.52, 131.30, 131.33 142.88, 195.54. Expected mass: 804.99 g/mol, ESI m/z = 822.87 $[M+NH_4]^+$.

2.2.5 Miktoarm star (**12**): 1 equivalent of compound **11** (0.4475 g, 0.556 mmol) was combined with 1.2 equivalents of lipoic acid (0.1376 g, 0.667 mmol) and DMAP (0.0815 g, 0.667 mmol) in a round bottom flask containing a stir bar, and 5 mL of dry DCM were added under argon. EDC (0.0862 g, 0.556 mmol) was added to the reaction mixture, and it was left to stir overnight under argon at room temperature. The resulting crude mixture was washed twice with MilliQ water and then dried over $MgSO_4$ before filtering. Finally the solvent was evaporated and column purification was performed using 3% MeOH in DCM, and a yellow oil was obtained upon subsequent removal of the solvent in vacuo (0.220 mg, 40% yield). ^{1}H NMR (400 MHz, $CDCl_3$): δ 1.45 (2H, dtdd, -C$\underline{H}_2$-), 1.60-1.73 (4H, m, -C$\underline{H}_2$-), 1.79-1.92 (1H, m, -SCHC$\underline{H}$H-), 2.26-2.30 (3H, m,-COC$\underline{H}_3$), 2.31-2.4 (3H, m, -C$\underline{H}_2$COO-, -SCHC$\underline{H}$H-), 3.02 (2H, t, C$\underline{H}_2$SCOCH$_3$), 3.06-3.19 (2H, m, -C$\underline{H}_2$SS-), 3.29-3.37 (3H, m, -$CH_2OC\underline{H}_3$), 3.52-3.67 (35H, m, -SSC$\underline{H}$-, C$\underline{H}_2$C$\underline{H}_2$O-), 3.92 (4H, ddd, -C$\underline{H}_2CH_2$triaz-), 4.60 (4H, ddt, -C$\underline{H}_2$triaz-), 5.18 (2H, d, -ArC$\underline{H}_2$O-), 7.82 (2H, dd, -Ar(C$\underline{H}$)-), 8.10 (2H, s, -triaz(CH)-), 8.21-8.27 (1H, m, -Ar(C$\underline{H}$)-). ^{13}C NMR (300MHz, $CDCl_3$): δ 24.64, 28.71, 28.75, 30.56, 34.02, 34.55, 38.45, 40.17, 50.48, 56.27, 59.01, 65.89, 69.47, 69.67, 70.26, 70.50-70.58, 71.88, 121.50, 122.67, 125.00, 131.69, 137.31, 146.91, 173.29, 195.48. Expected mass: 987.25 g/mol, ESI m/z =1009.67 $[M+Na]^+$.

2.3 Gold nanoshell synthesis: The method used was an adaptation of the synthetic procedure reported by Schwartzberg *et. al.*[1a] All glassware was cleaned with aqua regia (3:1 HCl:HNO_3) for minimum one hour followed by a number of ultra-pure water rinses, and dried in the oven. 1.5 L of MilliQ H_2O was placed in the 2L 3-necked round bottom flask and degassed rigorously to remove oxygen. Four cycles of the degassing procedure were carried out, where one cycle refers to placing the flask under vacuum, and then filling it with inert argon gas. Trisodium citrate (1.2345 g, 4.20 mmol) was added while the flask was kept under positive argon flow. The solution was degassed once more and filled with argon. It was followed by the addition of the cobalt (II) chloride hexahydrate (150.0g, 0.630 mmol), again under positive argon flow. The cobalt nanoparticles were formed when sodium borohydride ($NaBH_4$ – 142.5 mg, 3.77 mmol), dissolved in approximately 2 mL of degassed MilliQ H_2O, was added *via* syringe injection to the cobalt solution. A rapid color change to near-black indicated the formation of nanoparticles, while the presence of H_2 bubbles provided a visual cue for the completion of the reaction. Gold(III) chloride hydrate ($HAuCl_4$, 12.0 mg, 0.0353 mmol) was dissolved in a thrice degassed 900 mL of MilliQ H_2O placed in a 3L 3-necked round bottom flask. The cobalt solution, upon completion of the previous reaction (~1 hr), was rapidly transferred to the gold solution under argon flow. The crude mixture was reacted for 10 mins before opening to air for 4 hours for complete oxidation. The formation of GNS is accompanied by a green/grey color of the solution. The 2.4 L total volume was then concentrated by centrifugation in 50 mL tubes at 4600 rpm and 4ºC for 2 hours before removing the supernatants and recombining the separate pellets.

2.4 Conjugation of miktoarm star to gold nanoshells: In a typical conjugation process, 0.1 mmol of thioacetate protected ligand **12** was dissolved in 2 mL of dry MeOH under argon in a Schlenk flask. 1 equivalent of NaSMe (as a 1M solution in dry MeOH) was added dropwise, and the reaction was stirred at room temperature for 4h. It was then quenched by adding 2 mL of aqueous HCl (0.1 M), and the product extracted into DCM. The latter was washed with water and brine, and then dried over $MgSO_4$. The deprotected ligand was immediately reacted with the GNS solution concenterated to 1.5 mL in volume to which 2 drops of MeOH were added as a phase transfer agent to aid in solubility.

2.5 Cell culture and viability studies: HUVEC cells were cultured in fresh EBM2 medium (CC-3156, Lonza, MD, USA), supplemented with growth factors (CC-4176, Lonza, MD, USA) and incubated at 37^{o}C. Unless otherwise stated, all the cell culture experiments were performed by seeding HUVEC cells at a density of ~3x10^4 cells/cm^2. Viability assays of HUVEC cells were performed to determine the toxic effects of the miktoarm ligand, GNS and functionalized GNS. For the cytotoxic studies, cells were cultured overnight at 37^{o}C in 96-well plates and treated with various concentrations of GNS, functionalized GNS, miktoarm ligand, and LA. The concentrations of GNS and GNS-MA varied between 1 – 50 μg/mL for 24 and 48 h durations. The concentrations of the tri-

arm (0.25 to 8 μg/mL) and LA (0.05 to 1.67 μg/mL) as analyzed from TGA results (Table 1) were used for 24 or 48 h incubations. Interference between the GNS and the GNS-MA was assessed by addition of the assay reagents with the above concentration of nanoparticles and miktoarm stars but without cells. Cell viability was assessed using the CellTiter-Blue assay kit (G8080, Promega, WI, USA) according to the manufacturer instructions. CellTiter-Blue (20 μl) was added to each well 4 h before the end of each incubation duration and the plates were incubated at 37°C protected from light. The fluorescence was recorded on microplate reader (BioTek Synergy 2, USA) with excitation at 560 nm and emission at 590 nm.

2.6 Ultra-structural localization by transmission electron microscopy: Cells grown on 8-chamber plastic slides (Labtek, CA, USA) were exposed to various functionalized GNS, miktoarm ligands and LA concentrations for 12 h. The cells were then washed thrice with PBS and fixed in 2.5% electron microscopic grade glutaraldehyde prepared in 0.1 M phosphate buffered saline (PBS). Cells were then processed without staining using standard electron microscopy (EM) techniques. Briefly after the fixation, the fixed cell samples were placed in 2% osmium tetroxide with 0.1 M PBS, dehydrated in a graded series of ethyl alcohol, and embedded in Durcupan resin. Tissue blocks of the areas of interest were prepared and 80 nm ultrathin sections were cut with an ultramicrotome (Reichert-Jung UltracutE), which were then placed on formvar-coated slot copper TEM grids. The sections were then viewed with a FEI Tecnai BioTwinG^2 transmission electron microscope at 120 kV. Digital images were acquired with an AMT XR-60 CCD digital camera system.

2.7 Cell Internalization: Internalization of functionalized GNS was studied to determine the efficiency and rate of uptake by HUVEC cells. Cells were cultured in 10 cm^2 plates in EBM2 medium supplemented with growth factors. The cells were incubated overnight at 37°C, followed by addition of 50 (1.89 x 10^{10} GNS/mL) and 100 μg (3.79 x 10^{10} GNS/mL) of functionalized-GNS and incubated for 12, 24 and 48 h. At the end of each time point, the plates were thoroughly washed thrice with PBS to remove any unbound functionalized GNS. The cells were then trypsinized, centrifuged and the pellet was used for ICP-AES analysis.

2.8 Metal Content Analysis by Inductively-Coupled Plasma-Atomic Emission Spectroscopy (ICP-AES): ICP-AES analysis was performed to determine the cellular uptake of the functionalized GNS by quantifying the gold concentration. The cell pellets were digested with 70% nitric acid overnight, and the solution was diluted with Nano-Q water to make a 10% HNO_3 solution which was filtered through a 0.22 μm syringe filter. The ICP-OES was performed using an Optima 5300 ICP-OES spectrometer (Perkin-Elmer Inc, MA, USA). For each internalization study, the samples were measured 3 times for [Au] and the average calculated with its standard deviation by plotting a standard curve (0.1 to 50 μg/mL, R = 0.991) using λ_{max} = 242.795 nm.

For statistical analyses, all data are expressed as mean ± standard deviation (SD) (n=3, independent replicates). The statistical significance of difference between various treatment groups was analysed using Kruskal-Wallis test with Dunn post hoc. The statistical analysis was performed using SPSS with comparisons having $p<0.05$ considered to be significantly different.

3. Results and Discussion

3.1 Synthesis of miktoarm star ligand

The design of the miktoarm star ligand was based on a core building block which has orthogonal functional units, two individually protected acetylene groups and a benzylic hydroxyl group (**7**, Scheme **1**). It was synthesized starting from commercially available 3-bromo-5-iodo-benzoic acid, by first reducing it to the corresponding 3-bromo-5-iodo-benzyl alcohol, and subsequently carrying out Sonogoshira coupling to introduce protected acetylenes through bromo and iodo groups, sequentially.[8] The choice of the three arms to be coupled to the above building block was made based on their individual function: polyethylene glycol with a molecular weight of 350 (PEG_{350}) to introduce solubilizing and stealth capabilities, lipoic acid as a model therapeutic agent, and a thiol protected tetraethylene glycol (TEG-SAc) unit to couple the miktoarm star ligand to the GNS. To covalently link PEG_{350} to the core building block using highly efficient alkyne-azide "click" reaction, the hydroxyl end of PEG_{350} was first converted to a mesylate, followed by reaction with NaN_3 to yield azide terminated PEG_{350}.[19]

Tetraethylene glycol (TEG) is a shorter analog of polyethylene glycol and has been used extensively in nanoparticle functionalization.[22] It contains hydroxyl terminated ends, and for our purposes it was essential to introduce two orthogonal functionalities at these ends for "click" reaction to the core, and a thiol group for covalent linking to the GNS. To achieve this, p-toluenesulphonyl chloride was first reacted with TEG to form monotosylated-TEG.[19] To ensure that this reaction only occurs at one end of the TEG unit, a large excess of the sulphonyl reagent was required. To convert the tosylated end to a thiol, we attempted the reaction with thiourea, followed by hydrogenation with sodium hydroxide. It did yield the thiol terminated TEG, however, the free thiol was found to be unstable and quickly dimerized to give a disulphide bridged product. The free thiol group is also known to interfere with the click reaction of an alkyne with an azide in the presence of a copper catalyst. The protection of this free thiol was also attempted using Sanger's reagent (1-fluoro-2,4-dinitrobenzene).[23] The reaction proceeded smoothly, however, subsequent deprotection of it using excess mercaptoethanol or propane-thiol proved to be ineffective and led to impure products. We finally decided to use a protected thiol for the reaction which provided clean conversions yielding pure products. For this purpose, monotosylated-TEG was reacted with sodium thioacetate to replace the tosyl group with an acetate protected sulfur (TEG- SAc).[24]

Scheme **1**

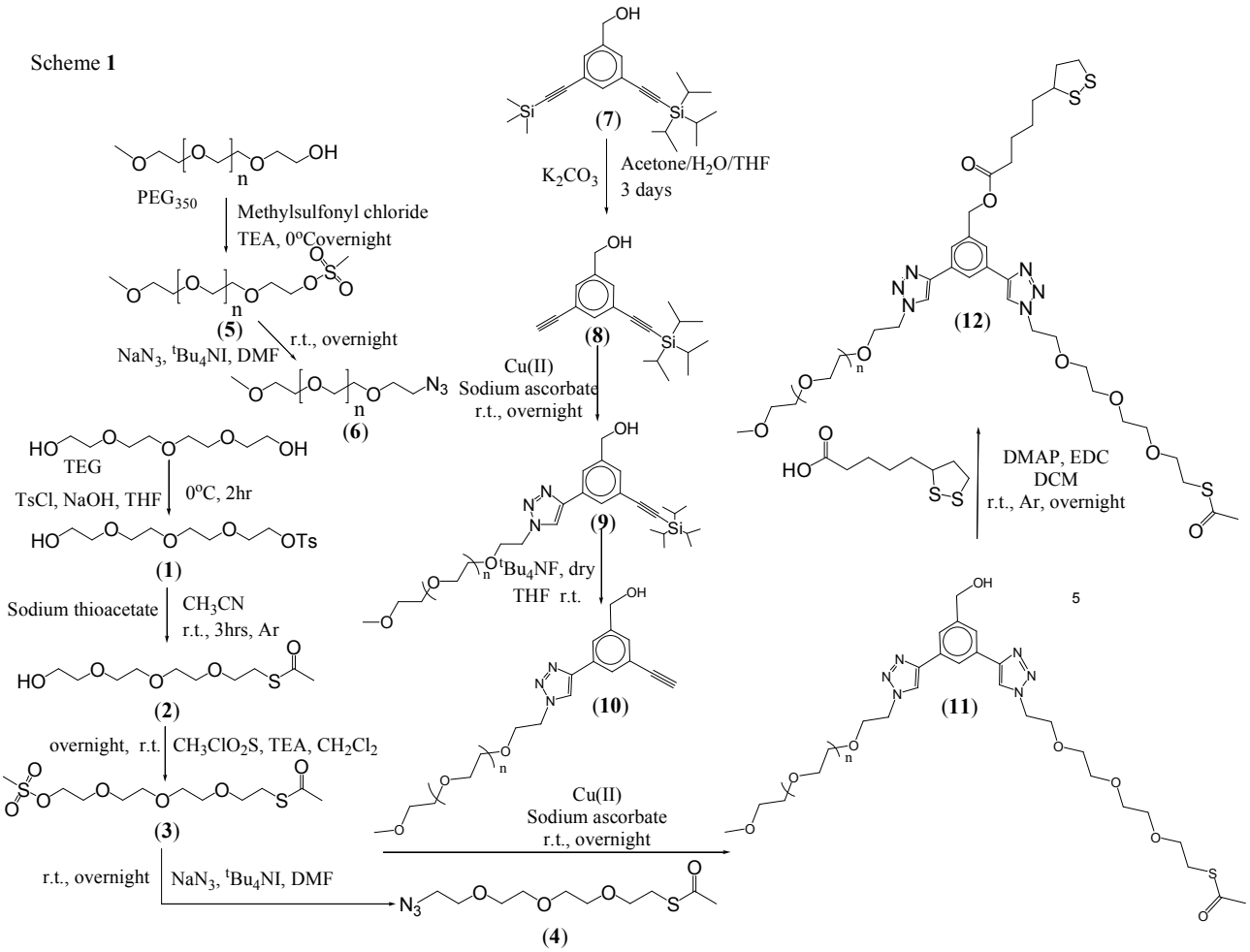

It was necessary to employ freshly prepared sodium thioacetate from sodium hydride and thioacetic acid, and add monotosylated-TEG dropwise to the thioacetate solution. The yellow-orange oil was found to be very sensitive to oxygen and turned brown on exposure to air. The azide functionality at the other end of TEG-SAc was then introduced using a similar procedure as described above for the azidation of PEG. TEG-SAc was first mesylated at the hydroxy end using methyl-sulphonyl chloride, and the product was then reacted with NaN_3 in the presence of tetrabutyl ammonium iodide at 50°C overnight. It led to the formation of sulfur protected TEG-azide (N_3-TEG-SAc) in a very good yield.

Miktoarm star (**12**, Scheme **1**) was constructed by stepwise introduction of different arms on to a building block. The trimethylsilyl end of one of the acetylenes on the core unit (**7**) was deprotected using potassium carbonate, yielding the free alkyne in a quantitative yield. It was noted that addition of THF to the acetone water mixture used in this reaction, expedited the reaction, as otherwise the reaction was found to be sluggish taking at least 2-3 days to complete. Azido-PEG_{350} was subsequently linked through the free alkyne using "click" chemistry, yielding the PEGylated core as colorless oil. The triisopropyl end group on the acetylene in the PEGylated core was then removed by reacting it with tetrabutylammonium fluoride. After removing excess THF in vacuum and an extraction with water, a clean product with free acetylene group was obtained. The latter was then employed to carry out the second "click" reaction with the azide terminated TEG-SAc, the column purification of which yielded the product in a good yield. The final step in the synthesis of the desired miktoarm star was the coupling of lipoic acid (LA) to the core unit through an esterification reaction. It is to be noted that the above mentioned sequence of events in the synthesis of the miktoarm star was necessary, as the thiol groups are known to interfere with click reaction. Once esterified, the product was purified on a column to yield a yellow oil which required storage under argon at 4 °C, as it was found to form a gel at room temperature.

3.2 Conjugation of miktoarm star to gold nanoshells

Gold nanoshells utilized in this study were synthesized using an adaptation of a previously reported procedure.[1a,4] It involved cobalt as a sacrificial template which was prepared by reducing cobalt(II) chloride hexahydrate with sodium borohydride, in the presence of a capping agent, trisodium citrate. The cobalt nanoparticles obtained from this reaction were added to a solution of aqueous aurochloric acid which oxidized cobalt. The reduced gold replaced cobalt on the outer surface, initiating the growth of a shell. A continuous flow of ion exchange enabled the movement of gold inward to replace cobalt with

Co(II) being diffused out, resulting in a hollow centre around which gold solidified into a shell.

The first step in the conjugation of the miktoarm star to GNS was the deprotection of TEG-SAc arm to yield the free thiol. The latter was carried out by reacting the tri-arm ligand with sodium methoxide in dry methanol at room temperature, under an inert atmosphere.[25] The reaction was then quenched with 0.1 M HCl. The deprotection was monitored by the disappearance of the acetate group associated peak using ^{1}H NMR. It should be noted that the product obtained should be used immediately for conjugation to gold as the formation of a disulfide linked dimer will occur otherwise.

The conjugation of the miktoarm star with the free thiol was carried out by stirring an aqueous solution of freshly synthesized and sonicated batch of GNS with the ligand. It has been suggested that the sulfur-gold conjugation can be enhanced by adjusting the pH of the solution to more basic conditions to remove the surface citrate ions from GNS.[26] However, when pH adjustment was attempted with our nanoshells, almost immediate aggregation of the nanoshells out of solution was observed.

The residual unconjugated miktoarm ligand was removed by two cycles of centrifugation of the solution at 2100 x g at 4ºC for 3 h.[27] After the first cycle, the nanoshell pellet was carefully removed, sonicated and transferred to a new centrifuge tube. This was done to prevent aggregation and adherence of the GNS to the centrifuge tube walls. The miktoarm ligand conjugated GNS did not aggregate even when standing for long periods, which confirmed their stability as a homogeneous solution.

3.3 Characterization of gold nanoshells before and after conjugation with mikotarm star ligand

Gold nanoshells were characterized using a combination of techniques including transmission electron microscopy (TEM), UV-Vis spectroscopy and thermogravimetric analysis (TGA). TEM analysis showed that the GNS are spherical with a hollow core, and an average shell diameter of ~40 nm and a thickness of ~3 nm (Figure 1a). After the miktoarm star ligand was grafted on to the GNS, there was no change in the overall shape, but the shell thickness was increased to 6 nm (Figure 1b), and the surface morphology was found to be rougher than the unfunctionalized GNS. EDS analysis showed characteristic peaks for gold (M_α and L_α at 2.12 and 9.17 keV) (Figure 1c, the Cu peak seen in the spectrum is from the TEM grid). High resolution TEM (HR-TEM) was subsequently carried out to see if the poly-crystallinity of the GNS had been altered after ligand grafting, as well as during purification and sonication steps. The HR-TEM of the GNS-miktoarm showed a polycrystalline structure with a number of single crystalline domains with different orientations, each with clear and well defined lattice fringes (representing individual atomic layers) separated by ~0.23 nm, and with large single areas of clear visible crystallinity. The lattice separation of 0.23 nm corresponds to the (111) lattice crystal plane for fcc-Au.[28]

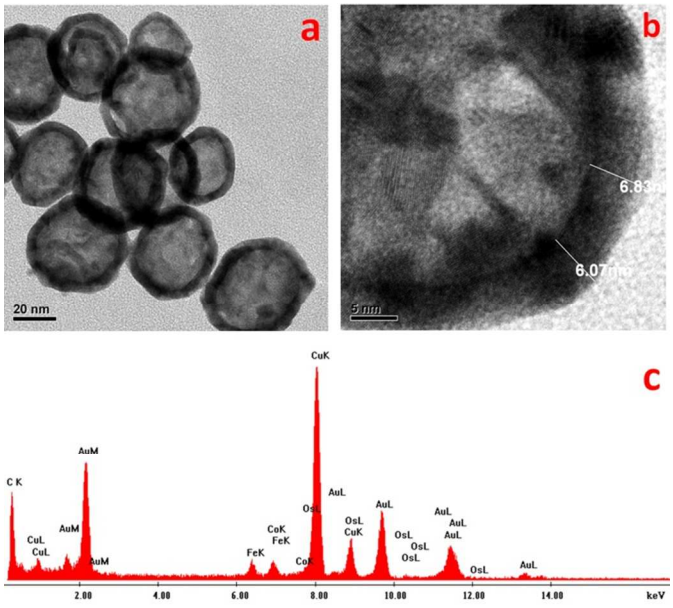

Figure **1**: (a) TEM image of the GNS; (b) HR-TEM image of the functionalized GNS (GNS-miktoarm) with the shell thickness; and (c) energy dispersive x-ray spectroscopy (EDS) analysis of GNS-miktoarm.

The surface plasmon properties of the GNS were studied by acquiring the absorption spectrum in the 400 – 800 nm range. The UV-Vis spectrum of the GNS before any functionalization, showed a strong absorption (λ_{max}) around 700 nm with a full-width half maximum (FWHM) of 5 nm (Figure 2a). The strong absorption suggests a complete shell formation,[29] and is confirmed by the TEM and EDX analyses. Functionalization with miktoarm star ligand did not affect the plasmon properties of GNS except for peak-broadening effect (Figure **2b**). The peak broadening may arise due to several factors such as polydispersity, presence of incompletely formed shells and roughness of the shell surface.[30] However, TEM analysis clearly showed that the GNS-miktoarm are monodisperse, and have completely formed shells. Thus, the peak broadening could be due to the covalent linking of the miktoarm unit onto the GNS surface.

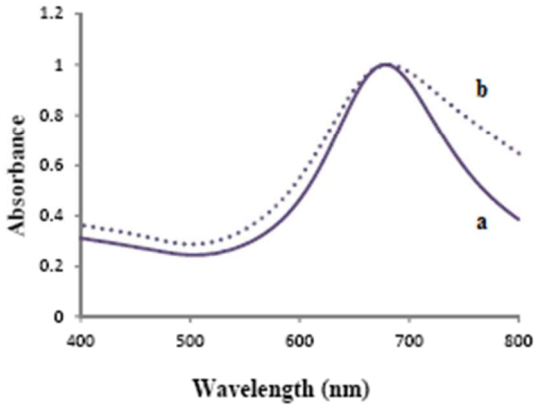

Figure **2**. UV-Vis absorption spectrum of (a) GNS and (b) functionalized GNS.

Thermogravimetric analyses of GNS before and after functionalization with the miktoarm ligand were performed (Figure S1), and their TGA profiles showed a weight loss onset at 163°C which proceeded up to 400°C in a 2 step manner, leaving a residue of 96% and 78%, respectively. The first step could account for the loss of adsorbed solvent molecules, and the second for the degradation of organic ligand. The TGA measurements revealed that miktoarm ligand constituted about 16% by weight of the ligand covering the GNS.

The number of miktoarm ligands bound to the GNS was calculated using Equation 3. Each GNS of 40 nm diameter and 3 nm shell thickness had ~807,765 atoms (N). The calculated molecular mass (M_{GNS} = N_{GNS} x M_{gold}) of each GNS is approximately 1.58 x 10^8 Da. From TGA analysis (16% of the gold dry mass), the number of miktoarm ligand molecules (Nt,) on each nanoshell was calculated to be ~12,377. The overall mass of GNS-miktoarm is thus 1.8 x 10^{10} Da (M_{GNS} + N_t * $M_{miktoarm}$ (= 945 Da)), and the packing density to be around 2.34 ligands/nm^2.

3.4 Cell viability studies

We carried out a detailed optical microscopy study upon treatment of cells with LA, miktoarm star, as well as GNS conjugated with this ligand (Figure 3). HUVEC cells before and after exposure to the free miktoarm ligand (0.25–8 μg/mL), and LA (0.05–1.67 μg/mL) showed no distinct morphological changes. Exposure of HUVEC cells to the miktoarm ligand at 8 μg/mL resulted in the formation of cellular clusters (as shown by the arrows, Figure 3, column IV – top panel). This behavior was not observed for the miktoarm ligand at lower doses or for LA at all the concentrations used in this study.

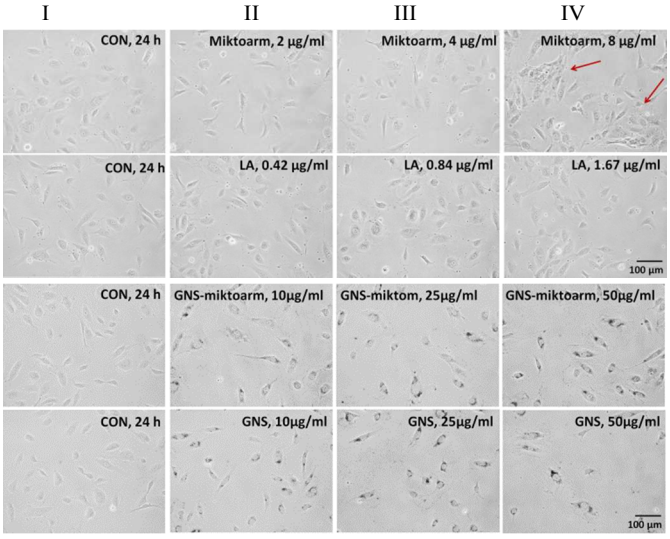

Figure **3**: Optical images of HUVEC cells treated with miktoarm ligand, LA, GNS and GNS-miktoarm at different concentrations for 24 h durations. Column I represents the untreated cells, column II – IV represents cells treated with indicated concentrations.

Gold nanoparticles have been shown to be cytotoxic in fibroblast, epithelial and melanoma cells,[31] unlike HeLa cells.[32] However, such studies are limited as there are numerous factors that remain unexplored, including the dependence of exposure time and surface functionalization. Cell viability assays can provide vital information about cytotoxicity, as well as cellular and metabolic activities. In order to determine the cytotoxic effects of miktoarm star ligand, and GNS before and after functionalization, CellTiter-Blue based viability assay was performed using HUVEC cells. This assay is a fluorescent based method that detects the mitochondrial activity based on the reduction of resazurin to resorufin in metabolically active cells.[33] In this study, we examined the time, surface functionalization and doses of the miktoarm functionalized GNS to evaluate their toxicity. The concentrations used for the miktoarm ligand (0.25 to 8 μg/mL) and LA (0.05 to 1.67 μg/mL) corresponded with the TGA results of 16% dry weight of the GNS. The concentrations for cell viability studies for functionalized GNS ranged from (1–50 μg/mL) (Table S1). Treatment with various concentrations of miktoarm ligand and LA did not affect the cell structure, and no altered cell morphology was observed (Figure 4). The results of the cell titer blue assay further confirmed that the metabolic activity of the cells did not change in the tested concentrations. This demonstrates that the miktoarm ligand and LA are biocompatible, and do not cause any structural and functional damage to the cells.

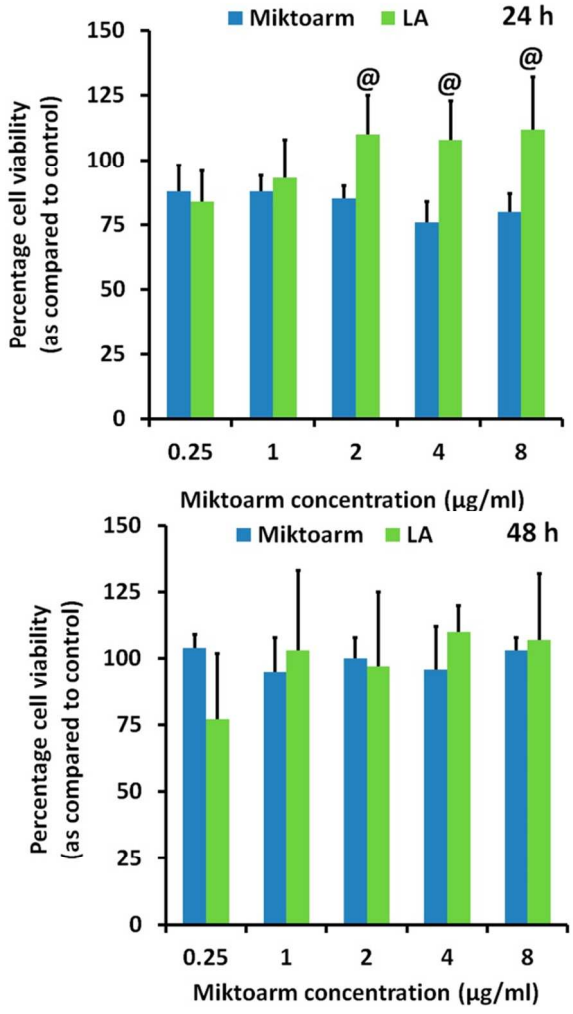

Figure **4**: Cell Titer-Blue assay to assess HUVEC cell viability after treatment with miktoarm ligand and LA at different concentrations for 24 (top) and 48 h (bottom). Data are presented as mean ± standard deviation (n=3 independent replicates). @p<0.05 is considered significant to miktoarm.

To assess the *in vitro* toxicity, we treated HUVEC cells with GNS before and after miktoarm ligand functionalization, in a concentration range of 1 – 50 µg/mL for 24 and 48 h (Figure 5). GNS before any functionalization did not cause any significant change in cell viability for up to 24 h at these concentrations (Figure 5). Treatment with functionalized GNS (GNS-miktoarm) at 10 µg/mL decreased the cell viability by ~50% as compared to the control (Figure 5), and to ~60% at 25 µg/mL. Increasing the GNS-miktoarm concentration beyond 25 µg/mL did not show any further reduction.

At 48 h, GNS treatment up to 10 µg/mL showed no significant change in the cell viability. Increasing the concentration to 25µg/mL reduced the cell viability to approximately 60%. Further increasing the concentration to 50 µg/mL did not reduce the cell viability. The results with functionalized GNS were similar to the 24h study, and there was ~50% reduction in cell viability at 10 µg/mL concentration.

The stability and functionalization of GNS plays a critical role in maintaining the cellular homeostasis, and depends on the molecular weight of PEG, functional groups, the overall molecular weight of the ligand, and the size of the GNS. Our results show that treatment with GNS and GNS-miktoarm up to 5 µg/mL causes no cytotoxicity in HUVEC cells for up to 48 h. Cytotoxicity was observed at or beyond 5 µg/mL concentrations after prolonged continuous exposure. One mechanism that could account for this is by altering the mitochondrial metabolic activity as analyzed by cell titer blue assay. Experimental evidence for such a phenomenon has been reported earlier.[34] We also observed that at 24 and 48 h time period there was no change in cell viability up to 5 µg/mL for both GNS and GNS-miktoarm treatment as compared to the control (Figure 5). It is hypothesized that this could be due to increase in the antioxidant defense enzymes which might have protected the cells from the enhanced pro-oxidants deleterious effects. Similar observations have been made earlier on gold nanoparticles containing PEG and biomolecules on their surface.[35]

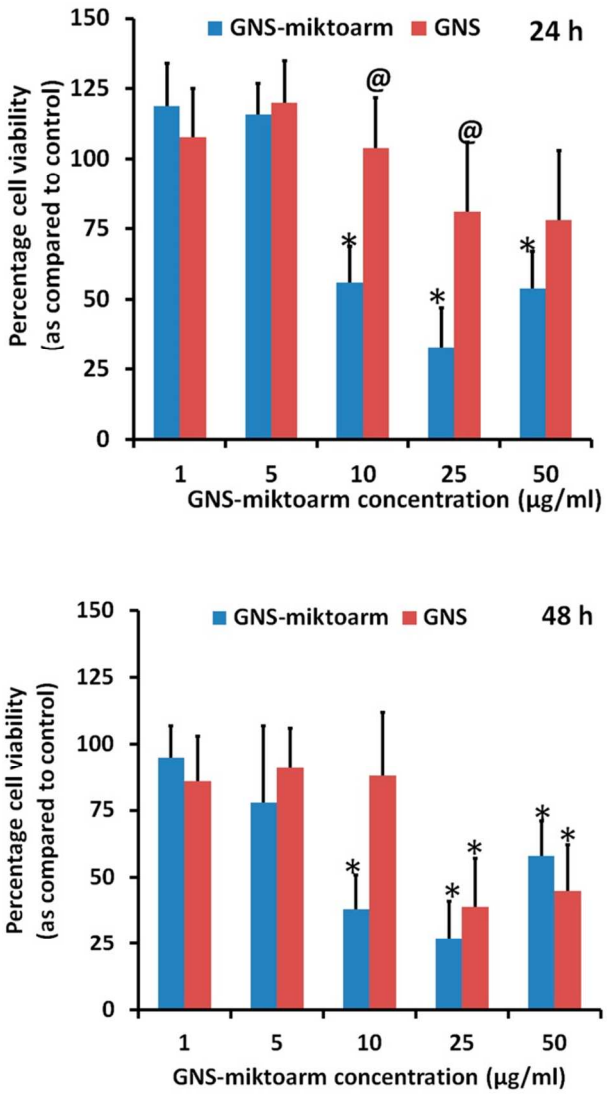

Figure **5**: Cell Titer-Blue assay to assess HUVEC cell viability after GNS and GNS-miktoarm treatment at different concentrations for 24h (top) and 48 h (bottom). Data are presented as mean ± standard deviation (n=3 independent replicates), * p<0.05 is considered significant as compared to control, @p<0.05 is considered significant to GNS-miktoarm.

3.5 Structural localization

The bio-distribution and localization of functionalized GNS in the HUVEC cells was examined using TEM (Figure 6). HUVEC cells showed no morphological changes before (Figure 6a,b) and after treatment with miktoarm-functionalized-GNS (Figure 6c-f). Functionalized GNS were found to accumulate in large numbers within endosomes (Figure 6c). At higher magnification these GNS were found as individual nanoshells of ~40 nm size in the endosomes (Figure 6d), and retained their original size and morphology within the cells, as evident from the shell structure indicated by the red arrows (Figure 6d).

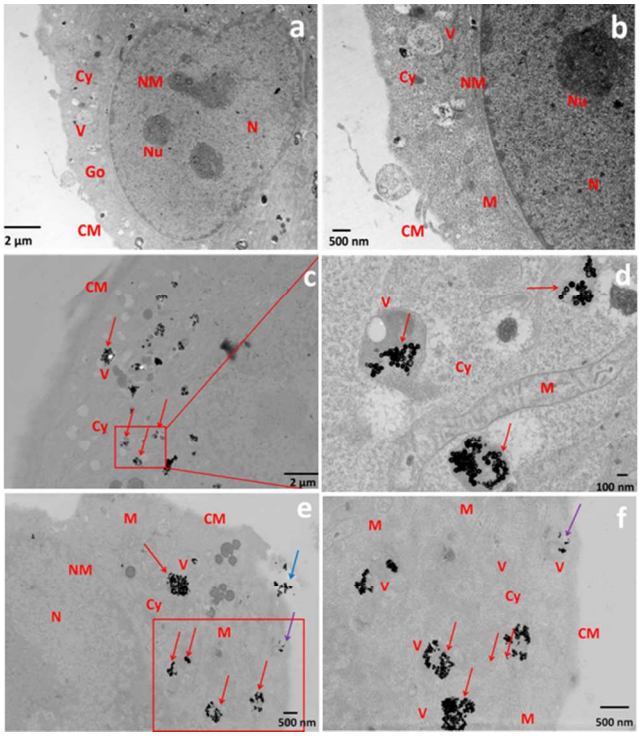

Figure **6**: Ultra-structural localization of GNS-miktoarm in HUVEC cells. TEM images of untreated (a,b) and treated cells (c-f) showing normal cellular morphology (a), a magnified region showing parts of the cytoplasm and nucleus (b), and cellular organelles: mitochondria (M), cytoplasm (Cy) cytoplasmic membrane (CM), nuclear membrane (NM), nucleus (N) and nucleolus (Nu). GNS-miktoarm uptaken are shown as red arrows in cells treated with 10 µg/mL for 24 h (c), and its magnified region (d). Panel c shows a large number of GNS endocytosed vacuoles (V). The image shows cytoplasm (Cy) with the GNS-miktoarm endocytosed vacuoles (red arrows). Magnified image (d) shows the endocytosed GNS-miktoarm localized only to the vacuoles and without any distribution in other cellular compartment. The areas showing the GNS endocytosed vacuoles are surrounded by mitochondria (M). HUVEC cells treated with 5 µg/mL of GNS-miktoarm for 24 h (e and f) also uptake GNS, though to a lesser extent. Panel e shows that GNS-miktoarm are uptaken through the process of endocytosis (blue arrow) where pseudopodia-like structures surround the GNS region. The purple arrow shows the GNS uptaken by early endosome near the membrane surface (f).

The endosomes containing functionalized GNS included small and large compartments that extended from 50 nm to as large as 1 µm (Figure 6e), and had diverse morphology that spread across the cytosolic as well as the membrane periphery (early and late endosomes) (Figure 6e,f). GNS before functionalization with the miktoarm star were also uptaken, but to a lower extent and seen as large aggregates (data not shown). The HR-TEM images show a clear distribution of individual miktoarm-functionalized-GNS in each endosomes that could be easily quantified visually (Figure S2 panels a and b).

TEM images clearly suggest that these functionalized-GNS are internalized by endocytosis, as evident by the endocytic vesicle formation (endocytic invaginations, blue arrows) around the functionalized GNS aggregates at the peripheral cell membrane (Figure 6 e,f). These images also showed that the miktoarm functionalized GNS were aggregated before being uptaken by the cells (Figure S3). This could be either due to the interaction of serum proteins (from the culture medium) with the GNS or interaction between the chains of the miktoarm ligand of various GNS that might have resulted in their aggregation before being uptaken by the cells. It has been reported[36] that serum albumin-coated nanoparticles of 100 nm size, larger than the size of caveolae, are easily uptaken by caveolae-mediated pathway, showing the flexibility and adaptability of the organelles (Figure S2a,b). This could be one of the mechanisms by which endocytosed-GNS aggregates of 1-3 µm in size could be seen in the HUVEC cells (Figure 6e). The other possibility might be that the GNS endocytosed vesicles might fuse to form larger sized vacuoles (Figure S2c). It has been suggested that the cellular uptake could be modulated by the aggregation state of nanoparticles.[37] Earlier, Chithrani et al. reported that 50 nm size transferrin-coated gold nanoparticles are easily uptaken as individual particles, as compared to the 14 nm size particles which were clustered before being uptaken by the cells.[38] It was also observed that GNS do not enter the nuclei, as the nuclear pores allow particles of size <9 nm by passive diffusion[39] and particles up to 40 nm by active diffusion.[40] Our results show that miktoarm functionalized GNS aggregates are uptaken through membrane invaginations larger than the size of caveolae. This leads to accumulation of these GNS in large amounts in the cells.

3.6 Cellular internalization characteristics of functionalized GNS

It is important to determine the concentration of functionalized GNS before treating them with the cells to understand the cellular internalization characteristics. Using ICP analysis, we estimated the solution concentration of gold to be 0.4 ppm. Considering the GNS average diameter of 40 nm and shell thickness of 3 nm, the number of GNS present in solution was calculated to be ~1.50 x 10^{12} GNS/mL (~400 µg/mL; 12 x 10^{17} gold atoms/mL) using equation (2). These samples were used to study the quantification of GNS internalized in HUVEC cells. Cells (1 x 10^{6}) were treated with 100 µg/10 mL [3.79 x 10^{11} GNS] and 50 µg/10 mL [1.89 x 10^{11} GNS] for 12, 24 and 48 h. At the end of each time period, ICP-AES was performed to quantitate the internalization of functionalized GNS into HUVEC cells. The results suggested that treatment with 50 µg (5µg/mL) of GNS-miktoarm for 12 h resulted in the uptake of approximately 1.6 x 10^{11} GNS-miktoarm (Supplementary Table 1). This indicates that the functionalized GNS are internalized with approximately 85% efficiency in the first 12 h. The uptake efficiency remained similar after prolonged treatment up to 48 h. Treatment with 100 µg resulted in reduced uptake efficiency of 45% at 12 h which increased up to 59% with incubation length of up to 24 h. However, the uptake efficiency dropped to 38% with prolonged exposure of GNS-miktoarm up to 48 h.

This indicates that treatment with 10^{10} GNS-miktoarm/mL is sufficient to achieve good internalization concentration within 12 h. It was reported earlier that gold nanoparticles of 25 nm size were internalized within 24 h into primary human dermal microvascular endothelial (HDMEC) and human cerebral microvascular endothelial cell lines (hCMEC/D3) with efficiencies of up to 5%.[7c,d] It is also known that bigger nanoshells are phagocytosed by macrophages more efficiently. A recent study also reported that PEGylated GNS with a size of 186 nm increased macrophage uptake to ~10%.[41]

Conclusions

A miktoarm ligand that is subsequently conjugated to GNS through one of its arms terminated with sulfur moiety has been synthesized, and evaluated as a platform for the development of functionally flexible GNS based probes. In this study, we covalently linked polyethylene glycol, lipoic acid and a TEGylated thiol, on to a building block with orthogonal functionalities. The use of "click" and esterification reactions demonstrates synthetic simplicity in the design of complex multi-tasking units, and facile incorporation of a desired combination of functional groups for imaging, circulation and therapeutic capabilities. The miktoarm star itself was found to be biocompatible, and did not change the morphology of HUVEC cells or their metabolic activity. Conjugation of the miktoarm ligand to GNS was easily achieved, and these functionalized GNS did not induce any change in the cellular morphology, and were easily uptaken by the cells. Miktoarm functionalized GNS (10μg/mL) were localized to endocytic vacuoles and retained their morphology for up to 48 h. The high uptake of functionalized GNS clearly suggests that a large number of pharmaceutical agents such as lipoic acid can be delivered to the cells. These results together with the versatility in introducing any desired combination of functional units into the miktoarm star composition, suggests that this is a promising methodology to develop highly efficient multifunctional nanocarriers with inherent imaging capabilities.

Acknowledgements

We would like to thank Natural Sciences and Engineering Research Council (Canada), Fonds de Recherche du Québec - Nature et technologies (FRQNT, Quebec, Canada), and Center for Self-assembled Chemical Structures (FQRNT, Quebec, Canada) for financial support.

Notes and references

[a] *Department of Chemistry, McGill University, 801 Sherbrooke St. West, Montreal, Quebec H3A 0B8 Canada. Fax: +514-398-3797; Tel: +514-398-6912; E-mail: ashok.kakkar@mcgill.ca*
[b] *Institute of Biomedical Engineering, École Polytechnique de Montréal, 2900, boul Édouard-Montpetit, Montreal, H3C 3A7, Canada Fax: 514-340-4611; Tel: +514-340-4711; E-mail: frederic.lesage@polymtl.ca*
[c] *Montreal Heart Institute, Research Center, 5000 Bélanger Est, Montréal, Quebec H1T 1C8, Canada Tel:+514-376-3330, ex. 3091. E-mail: Eric.Rheaume@icm-mhi.org*
[d] *Département de génie chimique et de génie biotechnologique, 2500, Boulevard Université, Université de Sherbrooke, Sherbrooke, Québec, J1K 2R1, Canada. Tel : +1-514-821-8000 ext . 62758. Email : Leonie.Rouleau@USherbrooke.Ca*
[e] *Département of Medicine, Université de Montréal, Montreal, Quebec, Canada*

†Electronic Supplementary Information (ESI) available: [details of any supplementary information available should be included here]. See DOI: 10.1039/b000000x/

‡These two authors made equal contributions.

1 (a) L. Rouleau, R. Berti, V. W. Ng, C. Matteau-Pelletier, T. Lam, P. Sabourla, A. K. Kakkar, F. Lesage, E. Rheaume, J. C. Tardif, *Contrast Media Mol Imaging*, 2013, 8(1), 27-39; (b) B. Panchapakesan, B. Book-Newell, P. Sethu, M. Rao, J. Irudayaraj, *Nanomedicine* 2011, 6 (10), 1787-1811; (c) E. Y. Lukianova-Hleb, A. O. Oginsky, A. P. Samaniego, D. L. Shenefelt, D. S. Wagner, J. H. Hafner, M. C. Farach-Carson, D. O. Lapotko, *Theranostics* 2011, 1, 3-17; (d) D. A. Giljohann, D. S. Seferos, W. L. Daniel, M. D. Massich, P. C. Patel, C. A. Mirkin, *Angew Chem Int Ed Engl* 2010, 49 (19), 3280-3294; (e) M. Hu, J. Chen, Z-Y. Li, L. Au, G. V. Hartland, X. Li, M. Marquez, Y. Xia, *Chem Soc Rev* 2006, 35 (11), 1084-1094; (f) C. Loo, A. Lowery, N. J. Halas, J. West, R. Drezek, *Nano Lett* 2005, 5 (4), 709-711; (g) J. Aizpurua, P. Hanarp, D. S. Sutherland, M. Kall, G. W. Bryant, F. J. G. de Abajo, *Phys Rev Lett* 2003, 90 (5), 057401-4; (h) L. R. Hirsch, R. J. Stafford, J. A. Bankson, S. R. Sershen, B. Rivera, R. E. Price, J. D. Hazle, N. J. Halas, J. L. West, *Proc. Nat Acad Sci, USA* 2003, 100 (23), 13549-13554).

2. (a) E. Prodan, P. Nordlander, N. J. Halas, *Nano Lett* 2003, 3, 1411; (b) R. D. Averitt, S. L. Westcott, N. J. Halas, *JOSA B* 1999, 16, 1824; (c) S. J. Oldenburg, S. L. Westcott, R. D. Averitt, N. J. Halas, *J. Chem Phys* 1999, 111, 4729.

3. (a) R. Averitt, D. Sarkar, N. J. Halas, *Phys Rev Lett* 1997, 78, 4217; (b) S. Oldenburg, R. Averitt, S. Westcott, N. Halas, *Cheml Phys Lett* 1998, 288, 243; (c) S. L. Westcott, S. J. Oldenburg, T. R. Lee, N. J. Halas, *Cheml Phys Lett* 1999, 300, 651; (d) Y. Sun, B. T. Mayers, Y. Xia, *Nano Lett* 2002, 2, 481; (e) H. P. Liang, H. M. Zhang, J. S. Hu, Y. G. Guo, L. J. Wan, C. L. Bai, *Angew Chem Int Ed Engl* 2004, 116, 1566; (f) H.-P. Liang, L.-J. Wan, C. L. Bai, L. Jiang, *J. Phys Chem B* 2005, 109, 7795.

4. A. M. Schwartzberg, T. Y. Olson, C. E. Talley, J. Z. Zhang, *J. Phys Chem B* 2006, 110, 19935.

5. J. Turkevich, P. C. Stevenson, J. Hillier, *Discuss Faraday Soc.* 1951, 11, 55.

6. (a) M.-C. Daniel, D. Astruc, *Chem Rev.* 2004, 104, 293; (b) G. B. Braun, A. Pallaoro, G. Wu, D. Missirlis, J. A. Zasadzinski, M. Tirrell, N. O. Reich, *ACS Nano* 2009, 3, 2007; (c) J. M. Slocik, F. Tam, N. J. Halas, R. R. Naik, R. R. *Nano Lett* 2007, 7, 1054; (d) S.-Y. Liu, Z.-S. Liang, F. Gao, S.-F. Luo, G.-Q. Lu, *J. Mater Sci Mater Med* 2010, 21, 665; (e) Z. Li, P. Huang, X. Zhang, J. Lin, S. Yang, B. Liu, F. Gao, P. Xi, Q. Ren, D. Cui, D. *Mol Phar* 2010, 7, 94; (f) G. Wu, A. Milkhailovsky, H. A. Khant, C. Fu, W. Chiu, J. A. Zasadzinski, *J. Am. Chem. Soc.* 2008, 130, 8175; (g) R. Bardhan, S. Lal, A. Joshi, N. J. Halas,. *Acc Chem Res* 2011, 44, 936; (h) D. A. Giljohann, D. S. Seferos, P. C. Patel, J. E. Millstone, N. L. Rosi, C. A. Mirkin, *Nano Lett* 2007, 7, 3818.

7. (a) I.-C. Lin, M. Liang, T.-Y. Liu, Z. M. Ziora, M. J. Monteiro, I. Toth, I. *Biomacromolecules* 2011, 12, 1339; (b) Z. Liang, Y. Liu, X. Li, Q. Wu, J. Yu, S. Luo, L. Lai, S. Liu, *J Biomed Mater Res A* 2011, 98, 479; (c) C. Freese, C. Uboldi, M. I. Gibson, R. E. Unger, B. B. Weksler, I. A. Romero, P. O. Couraud, C. J. Kirkpatrick, *Part Fibre Toxicol* 2012a, 9, 23; (d) C. Freese, M. I. Gibson, H. A. Klok, R. E. Unger, C. J. Kirkpatrick, *Biomacromolecules* 2012b, 13, 1533; (e) Z. J. Deng, M. Liang, I. Toth, M. J. Monteiro, R. F. Minchin, *ACS Nano* 2012, 6, 8962.
8. K. Khanna, S. Varshney, A. K. Kakkar, A. *Polymer Chem* 2010, 1, 1171.
9. (a) K. Khanna, S. Varshney, A. K. Kakkar, A. *Macromolecules* 2010, 43, 5688; (b) G. M. Soliman, R. Sharma, A. O. Choi, S. K. Varshney, F. M. Winnik, A. K. Kakkar, D. Maysinger, *Biomaterials* 2010, 31, 8382; (c) B. Iskin, G. Yilmaz, Y. Yagci, Y. *Polymer Chem* 2011, 2, 2865.
10. (a) V. V. Rostovtsev, L. G. Green, V. V. Fokin, K. B. Sharpless, *Angew Chemie Int Ed Engl* 2002, 114, 2708; (b) G. Franc, A. K. Kakkar, *Chem Soc Rev* 2010, 39, 1536; (c) G. M. Soliman, A. Sharma, D. Maysinger, A. K. Kakkar, *Chem Comm* 2011, 47, 9572.
11. (a) W.H. Binder and R. Sachsenhofer, *Macromol. Rapid Commun.* 2007, 28, 15; (b) S. Hvilsted, *Polym. Int.* 2012, 61 (4), 485; (c) P. K. Avti, D. Maysinger, A. Kakkar, A. *Molecules* 2013, 18, 9531.
12. (a) J. Davignon, P. Ganz, P. *Circulation* 2004, 109, 27; (b) L. F. Van Gaal, I. L. Mertens, C. E. De Block, *Nature* 2006, 444, 875; (c) Y. Taniyama, K. K. Griendling, Hypertension 2003, 42, 1075; (d) F. J. Miller, D. D. Gutterman, C. D. Rios, D. D. Heistad, B. L. Davidson, B. L. *Circ Res* 1998, 82, 1298.
13. S. D. Wollin, P. J. Jones, *J. Nutr.* 2003, 133, 3327.
14. L. J. Reed, B. B. De, I. C. Gunsalus, C. S. Hornberger, Jr. *Science* 1951, 114, 93.
15. (a) L. Packer, E. H. Witt, H. J. Tritschler, *Free Rad Biol Med* 1995, 19, 227; (b) K. P. Shay, R. F. Moreau, E. J. Smith, A. R. Smith, T. M. Hagen, *Biochim Biophys Acta* 2009, 1790, 1149.
16. (a) M. L. Bolognesi, A. Minarini, V. Tumiatti, C. Melchiorre, C. *Mini Rev Med Chem* 2006, 6, 1269.
17. B. Tharakan, J. G. Holder-Haynes, F. A. Hunter, E. W. Childs, E. W. *Am J Surg* 2008, 195, 174.
18. (a) J. C. Tardif, E. Rhéaume, E. *Br J Pharmacol* 2008, 153, 1587; (b) A. Smith, F. Visioli, B. Frei, T. Hagen, T. *British Journal of Pharmacology* 2008, 153, 1615; (c) S. Sola, M. Q. Mir, F. A. Cheema, N. Khan-Merchant, R. G. Menon, S. Parthasarathy, B. V. Khan, *Circulation* 2005, 111, 343; (d) Z. Ying, N. Kherada, B. Farrar, T. Kampfrath, Y. Chung, O. Simonetti, J. Deiuliis, R. Desikan, B. Khan, F. Villamena, Q. Sun, S. Parthasarathy, S. Rajagopalan, *Life Sci* 2010, 86, 95.
19. M.-C. Daniel, M. E. Grow, H. Pan, M. Bednarek, W. E. Ghann, K. Zabetakis, J. Cornish, *New J Chem* 2011, 35, 2366.
20. (a) H. Gao, K. Matyjaszewski, K. Journal of the American Chemical Society 2007, 129, 6633; (b) A. Sharma, G. M. Soliman, N. Al-Hajaj, R. Sharma, D. Maysinger, A. Kakkar, *Biomacromolecules* 2011, 13, 239.
21. (a) U. Lehmann, A. D. Schlüter, *European J Org Chem* 2000, 2000, 3483; (b) R. Hourani, A. Kakkar, A. *Macromol Rapid Commun* 2010, 31, 947.
22. M. Zheng, Z. Li, X. Huang, *Langmuir* 2004, 20, 4226.
23. G. Carrot, J. Hilborn, M. Trollsås, J. Hedrick, J. *Macromolecules* 1999, 32, 5264.
24. (a) R. Mahou and C. Wandrey, *Polymers*, 2012, 4, 561; (b) M.A. Petersen, L. Yin, E. Kokkoli, M.A. Hillmyer, *Polym. Chem.* 2010, **1**, 1281; (c) A. Balinski, M.Sc. Thesis, 2010, Vanderbilt University.
25. O. B. Wallace, D. M. Springer, *Tetrahedron Lett* 1998, 39, 2693.
26. Y. Zhou, S. Wang, K. Zhang, X. Jiang, *Angew Chemie Int Ed Engl* 2008, 47, 7454;
27. G. H. Woehrle, L. O. Brown, J. E. Hutchison, *J Am Chem Soc* 2005, 127, 2172.
28. L. Zhu, G. Lu, J. Chen, J. Journal of Heat Transfer 2008, 130, 44502.
29. C. Graf, and A. van Blaaderen, A. *Langmuir* 2002, 18, 524.
30. (a) S. Oldenburg, G. Hale, J. Jackson, N. J. Halas, *Appl Phys Lett* 1999, 75, 1063; (b) S. J. Oldenburg, J. B. Jackson, S. L. Westcott, N. J. Halas, *Appl Phys Lett* 1999, 75, 2897.
31. Y. Pan, S. Neuss, A. Leifert, M. Fischler, F. Wen, U. Simon, G. Schmid, W. Brandau, W. Jahnen-Dechent, *Small* 2007, 3, 1941.
32. (a) T. S. Hauck, A. A. Ghazani, W. C. Chan, W. C. *Small* 2008, 4, 153; (b) J. A. Khan, B. Pillai, T. K. Das, Y. Singh, S. Maiti, S. *Chembiochem* 2007, 8, 1237.
33. J. O'Brien, I. Wilson, T. Orton, F. Pognan, *Eur J Biochem* 2000, 267, 5421.
34. T. C. Long, N. Saleh, R. D. Tilton, G. V. Lowry, B. Veronesi, B. *Envir Sci Technol* 2006, 40, 4346.
35. (a) Z. Mao, B. Wang, L. Ma, C. Gao, J. Shen, *J. Nanomedicine* 2007, 3, 215; (b) H.K. Patra, S. Banerjee, U. Chaudhuri, P. Lahiri, A. K. Dasgupta, A. K. *Nanomedicine* 2007, 3, 111; (c) A. S. Thakor, R. Paulmurugan, P. Kempen, C. Zavaleta, R. Sinclair, T. F. Massoud, S. S. Gambhir, S. S. *Small* 2011, 7, 126; (d) W.-S. Cho, M. Cho, J. Jeong, M. Choi, H.-Y. Cho, B. S. Han, S. H. Kim, H. O. Kim, Y. T. Lim, B. H. Chung, B. H. *Toxicol Appl Pharmacol* 2009, 236, 16; (e) Y.-S. Chen, Y.-C. Hung, I. Liau, G. S. Huang, *Nanoscale Res Lett* 2009, 4, 858; (f) S.-M. Ryou, S. Kim, H. H. Jang, J. H. Kim, J.-H. Yeom, M. S. Eom, J. Bae, M. S. Han, K. Lee, K. *Biochem Biophys Res Commun* 2010, 398, 542; (g) M. D. Massich, D. A Giljohann, A. L; Schmucker, P. C. Patel, C. A. Mirkin, *ACS Nano* 2010, 4, 5641; (h) J. Conde, J. de la Fuente, P. Baptista, P. *Nanotechnology* 2010, 21, 505101; (i) C. Uboldi, D. Bonacchi, G. Lorenzi, M. I. Hermanns, C. Pohl, G. Baldi, R. E. Unger, C. Kirkpatrick, *J. Part Fibre Toxicol* 2009, 6, 18.
36. Z. Wang, C. Tiruppathi, R. D. Minshall, A. B. Malik, A. B. *ACS Nano* 2009, 3, 4110.
37. J. B. Hall, M. A. Dobrovolskaia, A. K. Patri, S. E. McNeil, *Nanomedicine (Lond)* 2007, 2, 789.
38. B. Chithrani, W. C. Chan, *Nano Lett* 2007, 7, 1542.
39. H. S. Choi, W. Liu, P. Misra, E. Tanaka, J. P. Zimmer, B. Itty Ipe, M. G. Bawendi, J. V. Frangioni, *Nat Biotechnol* 2007, 25, 1165.
40. N. Pante, and M. Kann, *Mol Biol Cell* 2002, 13, 425.
41. J.C. Kah, K. Y. Wong, K. G. Neoh, J. H. Song, J. W. Fu, S. Mhaisalkar, M. Olivo, C. J. Sheppard, *J Drug Target* 2009, 17, 181.

Table of Contents Entry:

Miktoarm star conjugated multifunctional gold nanoshells: synthesis and an evaluation of biocompatibility and cellular uptake

Vanessa W.K. Ng, Pramod K. Avti, Mathieu Bedard, Tina Lam, Leonie Rouleau, Jean-Claude Tardif, Eric Rhéaume,* Frederic Lesage* and Ashok Kakkar*

Biocompatible multifunctional gold nanoshells with imaging, stealth/aqueous solubility and therapeutic capabilities show high accumulation into endothelial cells.